

## Mixing of valence subbands in GaAs/Al<sub>x</sub>Ga<sub>1-x</sub>As multiple quantum wells by uniaxial stress

Johnson Lee, C. Jagannath, M. O. Vassell, and Emil S. Koteles  
*GTE Laboratories, Incorporated, 40 Sylvan Road, Waltham, Massachusetts 02254*  
 (Received 7 July 1987)

The effects of uniaxial stress on the energies of exciton transitions in GaAs/Al<sub>x</sub>Ga<sub>1-x</sub>As multiple quantum wells are investigated both theoretically and experimentally. The valence subbands and the corresponding wave functions are analyzed at the Brillouin-zone center by solving a 4×4 Luttinger-Kohn Hamiltonian in conjunction with a 4×4 strain Hamiltonian in the spin  $J = \frac{3}{2}$  basis. Appropriate boundary conditions are obtained by integrating the total Hamiltonian across the interfaces of the wells. Good agreement is obtained between numerical calculations on a 22-nm-wide quantum well subjected to a uniaxial stress in the plane of the well and experimental results obtained using photoluminescence excitation spectroscopy at liquid-helium temperatures. Evidence of valence-subband mixing between the light-hole exciton and higher levels of heavy-hole excitons is clearly observed.

### I. INTRODUCTION

The optical properties of a semiconductor quantum-well (QW) structure exhibit many unique characteristics which differ from those of the bulk constituents. For example, the binding energy of excitons increase as a result of two-dimensional confinement. Consequently exciton absorption persists, and has been observed at room temperature.<sup>1,2</sup> Another interesting feature of the structure is the observation of forbidden exciton transitions<sup>3</sup> which have been interpreted in terms of valence-band mixing. The oscillator strengths of these "forbidden" transitions become large when the energy of the valence subband involved is close to that of another valence subband which participates in an allowed transition as a consequence of shifts of valence-subband energies due to spatial confinement effects.<sup>3-6</sup> Since, in the Luttinger-Kohn formalism, all off-diagonal elements in the Hamiltonian are zero at the zone center,  $k=0$  (where  $k$  is the wave vector describing the relative motion of the electron and holes parallel to the interface of the quantum well), the observation of parity forbidden transitions is attributed to direct transitions between states situated away from the zone center ( $k \neq 0$ ). However, if uniaxial compression or tension is applied parallel to the plane of the quantum wells,<sup>7</sup> off-diagonal elements of the total Hamiltonian, which is a sum of the Luttinger-Kohn and the strain Hamiltonians, can be nonzero, even at  $k=0$ , leading to valence-band mixing. Using externally applied uniaxial stress, the coincidence of the valence-subband states can be brought about in a precisely controllable and reproducible manner. Since the magnitude of the interaction can be tuned and precisely controlled in this way, a detailed comparison between experiment and theory is possible.

In this paper we examine, both theoretically and experimentally, the effects of uniaxial stress on excitons in quantum wells at  $k=0$ . In Sec. II, a theoretical model is presented which can be used to calculate the eigenenergies and the corresponding eigenfunctions of the total Hamiltonian. In Sec. III, we describe our experimental

technique and results of uniaxial stress experiments on a 22-nm-wide GaAs/Al<sub>x</sub>Ga<sub>1-x</sub>As QW. Finally, in Sec. IV we discuss our numerical results and compare them with our experimental results.

### II. THEORETICAL MODEL

In our theoretical model, semiconductor quantum wells were taken to have a finite depth ( $V_e$  in the conduction band and  $V_h$  in the valence band) and assumed to experience an external compressive uniaxial stress  $X$  along an arbitrary direction. A confined exciton is then described by a Hamiltonian<sup>8</sup>  $\underline{H}_t$ , containing the Luttinger-Kohn Hamiltonian  $\underline{H}$  (with the Coulombic electron-hole interaction included) plus the strain Hamiltonian<sup>9</sup>  $\underline{H}_\epsilon$ . In a spin- $\frac{3}{2}$  basis for a valence band without spin-orbit interaction and in a spin- $\frac{1}{2}$  basis for the conduction band,  $\underline{H}$  and  $\underline{H}_\epsilon$  are 4×4 matrices (in atomic units) with matrix elements  $H_{ij}$  and  $H_{ij}^\epsilon$ ,  $i, j = 1, 2, 3, 4$ :

$$\underline{H}_t = \underline{H} + \underline{H}_\epsilon, \tag{1}$$

$$\underline{H} = \begin{pmatrix} H_{11} & H_{12} & H_{13} & 0 \\ H_{12}^* & H_{22} & 0 & -H_{13} \\ H_{13}^* & 0 & H_{22} & H_{12} \\ 0 & -H_{13}^* & H_{12}^* & H_{11} \end{pmatrix}, \tag{2}$$

$$H_{11} = \left[ (\gamma_0 + \gamma_1 + \gamma_2)k^2 - \frac{2}{[\rho^2 + (z - z')^2]^{1/2}} \right] + \gamma_0 k_z^2 + (\gamma_1 - 2\gamma_2)k_z^2, \tag{3}$$

$$H_{22} = \left[ (\gamma_0 + \gamma_1 - \gamma_2)k^2 - \frac{2}{[\rho^2 + (z - z')^2]^{1/2}} \right] + \gamma_0 k_z^2 + (\gamma_1 + 2\gamma_2)k_z^2, \tag{4}$$

$$H_{12} = \sqrt{3}[\gamma_2(k_x^2 - k_y^2) - i2\gamma_3 k_x k_y], \quad (5)$$

$$H_{13} = -i2\sqrt{3}\gamma_3 k_z(k_x - ik_y), \quad (6)$$

and

$$\underline{H}_\epsilon = \begin{pmatrix} H_{11}^\epsilon & H_{12}^\epsilon & H_{13}^\epsilon & 0 \\ H_{12}^{\epsilon*} & H_{22}^\epsilon & 0 & -H_{13}^\epsilon \\ H_{13}^{\epsilon*} & 0 & H_{22}^\epsilon & H_{12}^\epsilon \\ 0 & -H_{13}^{\epsilon*} & H_{12}^{\epsilon*} & H_{11}^\epsilon \end{pmatrix}, \quad (7)$$

$$H_{11}^\epsilon = (D_d + C_1)(\epsilon_{xx} + \epsilon_{yy} + \epsilon_{zz}) + \frac{2}{3}D_u[\epsilon_{zz} - \frac{1}{2}(\epsilon_{xx} + \epsilon_{yy})], \quad (8)$$

$$H_{22}^\epsilon = (D_d + C_1)(\epsilon_{xx} + \epsilon_{yy} + \epsilon_{zz}) - \frac{2}{3}D_u[\epsilon_{zz} - \frac{1}{2}(\epsilon_{xx} + \epsilon_{yy})], \quad (9)$$

$$H_{12}^\epsilon = \frac{D_u}{\sqrt{3}}(\epsilon_{yy} - \epsilon_{xx}) + i\frac{2}{\sqrt{3}}D_u'\epsilon_{xy}, \quad (10)$$

$$H_{13}^\epsilon = \frac{2}{\sqrt{3}}D_u'(\epsilon_{yz} + i\epsilon_{zx}). \quad (11)$$

In the above, the Luttinger parameters are  $\gamma_0$  (for the conduction band), and  $\gamma_1$ ,  $\gamma_2$ , and  $\gamma_3$  (for the valence band); the deformation potentials are  $C_1$  (for the conduction band), and  $D_d$ ,  $D_u$ , and  $D_u'$  (for the valence band);  $\epsilon_{ij}$ ,  $i, j = x, y, z$ , is the strain tensor; and

$$\mathbf{k} = -i\nabla_\rho, \quad k_z = -i\partial/\partial z, \quad k_z' = -i\partial/\partial z'$$

are operators.  $\rho$  is the relative displacement of the electron and hole in the  $x$ - $y$  plane, and  $z$  ( $z'$ ) is the projection of the position vector of the hole (electron) on the  $z$  axis (the spatial quantization axis due to confinement). The total Hamiltonian  $\underline{H}_t$  contains the confinement potential-energy functions for electron,

$$V_e(z') = \begin{cases} V_e & \text{if } |z'| \leq L/2 \\ 0 & \text{if } |z'| > L/2 \end{cases} \quad (12)$$

and, for holes,

$$V_h(z) = \begin{cases} V_h & \text{if } |z| \leq L/2 \\ 0 & \text{if } |z| > L/2, \end{cases} \quad (13)$$

where  $L$  is the quantum-well width. In the barrier regions, i.e.,  $|z| > L/2$  and  $|z'| > L/2$ , the Luttinger parameters  $\gamma_0$ ,  $\gamma_1$ ,  $\gamma_2$ , and  $\gamma_3$  must be replaced by those appropriate to the material of the barrier,  $\gamma'_0$ ,  $\gamma'_1$ ,  $\gamma'_2$ , and  $\gamma'_3$ . For a GaAs/Ga<sub>1-x</sub>Al<sub>x</sub>As quantum well, the  $x$  dependences of  $V_e$ ,  $V_h$ , and  $\gamma'_i$  are given by<sup>10-12</sup>

$$\begin{aligned} V_e &= 70\%[x(1.155 + 0.37x)]\text{eV}, \\ V_h &= 30\%[x(1.155 + 0.37x)]\text{eV}, \\ \gamma'_0(x) &= \gamma_0 - 13.52x, \\ \gamma'_1(x) &= \gamma_1 - 3.40x, \\ \gamma'_2(x) &= \gamma_2 - 1.42x, \\ \gamma'_3(x) &= \gamma_3 - 1.61x, \end{aligned} \quad (14)$$

where the numerical values of the Luttinger parameters appropriate for GaAs (Ref. 10) are  $\gamma_0 = 14.925$ ,  $\gamma_1 = 6.85$ ,  $\gamma_2 = 2.1$ , and  $\gamma_3 = 2.9$ .

It is difficult to solve the eigenvalue problem for Eqs. (1)–(13) directly. However, most experiments probe exciton effects near  $k=0$ , where  $H_{12}$  [Eq. (5)] and  $H_{13}$  [Eq. (6)] are small. Therefore, we assume that  $H_{12}$  and  $H_{13}$  are negligible and, further, that the quantities in the large parentheses in Eqs. (3) and (4) may be replaced by the binding energy of the heavy-hole exciton,  $E_{b1}$ , and the binding energy of the light hole exciton,  $E_{b2}$ , respectively. Then we obtain the following simplified matrix elements for the total Hamiltonian:

$$\begin{aligned} H_{t11} &= \gamma_0 k_z'^2 + \Upsilon_1 k_z^2 + E_{b1} + H_{11}^\epsilon, \\ H_{t22} &= \gamma_0 k_z'^2 + \Upsilon_2 k_z^2 + E_{b2} + H_{22}^\epsilon, \\ H_{t12} &= H_{12}^\epsilon, \quad H_{t13} = H_{13}^\epsilon, \end{aligned} \quad (15)$$

with

$$\Upsilon_1 = \gamma_1 - 2\gamma_2, \quad \Upsilon_2 = \gamma_1 + 2\gamma_2,$$

where  $\underline{H}_t$  has the same form as in Eq. (2). If uniaxial stress  $X$  is applied in the [100] or [001] directions, the strain matrix element  $H_{13}^\epsilon$  is zero, and the  $4 \times 4$  matrix  $\underline{H}_t$  is reduced to two identical  $2 \times 2$  matrices. We only need to solve a coupled differential equation

$$\begin{bmatrix} -\Upsilon_1 \partial_z^2 + V_h(z) + E_c + E_{b1} + H_{11}^\epsilon - E & H_{12}^\epsilon \\ H_{12}^\epsilon & -\Upsilon_2 \partial_z^2 + V_h(z) + E_c + E_{b2} + H_{22}^\epsilon - E \end{bmatrix} \begin{bmatrix} \psi_1(z) \\ \psi_2(z) \end{bmatrix} = 0 \quad (16)$$

with

$$[-\gamma_0 \partial_z^2 + V_e(z')]\varphi(z') = E_c \varphi(z'), \quad (17)$$

where  $E$  is the total energy of the system,  $E_c$  is the conduction subband energy, and  $\varphi(z')$  and  $\psi_i(z)$  are the envelope functions of the conduction band and valence bands, respectively. The boundary conditions are obtained by integrating Eqs. (16) and (17) across the interfaces of the quantum well at  $z = \pm L/2$  and  $z' = \pm L/2$ . Equation (16) yields the boundary conditions

$$\begin{aligned} \Upsilon_1 \psi_1 \left[ \pm \frac{L}{2} \mp \delta \right] &= \Upsilon_1' \psi_1 \left[ \pm \frac{L}{2} \pm \delta \right], \\ \Upsilon_2 \psi_2 \left[ \pm \frac{L}{2} \mp \delta \right] &= \Upsilon_2' \psi_2 \left[ \pm \frac{L}{2} \pm \delta \right], \\ \psi_1 \left[ \pm \frac{L}{2} \mp \delta \right] &= \psi_1 \left[ \pm \frac{L}{2} \pm \delta \right], \\ \psi_2 \left[ \pm \frac{L}{2} \mp \delta \right] &= \psi_2 \left[ \pm \frac{L}{2} \pm \delta \right] \end{aligned} \quad (18)$$

for the valence bands, while Eq. (17) produces the conditions

$$\begin{aligned} \gamma_0 \varphi' \left[ \pm \frac{L}{2} \mp \delta \right] &= \gamma_0' \varphi' \left[ \pm \frac{L}{2} \pm \delta \right], \\ \varphi \left[ \pm \frac{L}{2} \mp \delta \right] &= \varphi \left[ \pm \frac{L}{2} \pm \delta \right] \end{aligned} \tag{19}$$

for the conduction band. Here, the prime in  $\varphi'(z')$  and  $\psi'_i(z)$  represents the partial differential with respect to  $z'$  and  $z$ , respectively, and  $\delta$  is an infinitesimal. The solutions of Eq. (17) with the boundary conditions of Eqs. (19) are well known<sup>13</sup> and are given by

$$\varphi(z') = \begin{cases} W_1 \cos(qz') & \text{if } 0 \leq z < L/2 \\ B_1 e^{-\kappa z'} & \text{if } L/2 \leq z < \infty, \end{cases} \tag{20}$$

$$\tan(qL/2) = \gamma_0' \kappa / \gamma_0 q$$

if  $\varphi$  is an even function of  $z'$ , and by

$$\varphi(z') = \begin{cases} W_2 \sin(qz') & \text{if } 0 \leq z < L/2 \\ B_2 e^{-\kappa z'} & \text{if } L/2 \leq z < \infty, \end{cases} \tag{21}$$

$$\cot(qL/2) = -\gamma_0' \kappa / \gamma_0 q$$

if  $\varphi$  is an odd function of  $z'$ . Quantities  $q$  and  $\kappa$  are defined as  $(E_c/\gamma_0)^{1/2}$  and  $[(V_e - E_c)/\gamma_0']^{1/2}$ , respectively, and  $W_j, B_j, j=1,2$ , are constants. To obtain the solutions for Eq. (16) with the boundary conditions Eq. (18), we follow the scheme proposed by Nedorezov<sup>14</sup> and summarized below. If  $\psi_i(z)$  is an even function of  $z$ , we write

$$\begin{aligned} \begin{pmatrix} \psi_1(z) \\ \psi_2(z) \end{pmatrix} &= \begin{pmatrix} W_1 \Lambda_1 \cos(q_1 z) + W_3 \Lambda_2 \cos(q_2 z) \\ W_1 \cos(q_1 z) + W_3 \cos(q_2 z) \end{pmatrix} \\ &\text{if } 0 \leq z < L/2 \end{aligned} \tag{22}$$

$$\begin{aligned} \begin{pmatrix} \psi_1(z) \\ \psi_2(z) \end{pmatrix} &= \begin{pmatrix} B_1 \Lambda_1' e^{-\kappa_1 z} + B_3 \Lambda_2' e^{-\kappa_2 z} \\ B_1 e^{-\kappa_1 z} + B_3 e^{-\kappa_2 z} \end{pmatrix} \\ &\text{if } L/2 \leq z < \infty. \end{aligned}$$

Then the boundary conditions yield

$$\begin{pmatrix} \Lambda_1 \cos(q_1 L/2) & \Lambda_2 \cos(q_2 L/2) & -\Lambda_1' & -\Lambda_2' \\ \cos(q_1 L/2) & \cos(q_2 L/2) & -1 & -1 \\ -q_1 \Lambda_1 \Upsilon_1 \sin(q_1 L/2) & -q_2 \Lambda_2 \Upsilon_1 \sin(q_2 L/2) & \kappa_1 \Lambda_1' \Upsilon_1' & \kappa_2 \Lambda_2' \Upsilon_1' \\ -q_1 \Upsilon_2 \sin(q_1 L/2) & -q_2 \Upsilon_2 \sin(q_2 L/2) & \kappa_1 \Upsilon_2' & \kappa_2 \Upsilon_2' \end{pmatrix} \begin{pmatrix} W_1 \\ W_3 \\ e^{-\kappa_1 L/2} B_1 \\ e^{-\kappa_2 L/2} B_3 \end{pmatrix} = 0. \tag{23}$$

But if  $\psi_i(z)$  is an odd function of  $z$ , we have

$$\begin{aligned} \begin{pmatrix} \psi_1(z) \\ \psi_2(z) \end{pmatrix} &= \begin{pmatrix} W_2 \Lambda_1 \sin(q_1 z) + W_4 \Lambda_2 \sin(q_2 z) \\ W_2 \sin(q_1 z) + W_4 \sin(q_2 z) \end{pmatrix} \\ &\text{if } 0 \leq z < L/2 \\ \begin{pmatrix} \psi_1(z) \\ \psi_2(z) \end{pmatrix} &= \begin{pmatrix} B_2 \Lambda_1' e^{-\kappa_1 z} + B_4 \Lambda_2' e^{-\kappa_2 z} \\ B_2 e^{-\kappa_1 z} + B_4 e^{-\kappa_2 z} \end{pmatrix} \\ &\text{if } L/2 \leq z < \infty. \end{aligned} \tag{24}$$

Then the boundary conditions become

$$\begin{pmatrix} \Lambda_1 \sin(q_1 L/2) & \Lambda_2 \sin(q_2 L/2) & -\Lambda_1' & -\Lambda_2' \\ \sin(q_1 L/2) & \sin(q_2 L/2) & -1 & -1 \\ q_1 \Lambda_1 \Upsilon_1 \cos(q_1 L/2) & q_2 \Lambda_2 \Upsilon_1 \cos(q_2 L/2) & \kappa_1 \Lambda_1' \Upsilon_1' & \kappa_2 \Lambda_2' \Upsilon_1' \\ q_1 \Upsilon_2 \cos(q_1 L/2) & q_2 \Upsilon_2 \cos(q_2 L/2) & \kappa_1 \Upsilon_2' & \kappa_2 \Upsilon_2' \end{pmatrix} \begin{pmatrix} W_2 \\ W_4 \\ e^{-\kappa_1 L/2} B_2 \\ e^{-\kappa_2 L/2} B_4 \end{pmatrix} = 0, \tag{25}$$

where  $W_i$  and  $B_i, i=1,2,3,4$ , are amplitudes of the envelope functions and  $q_j, \kappa_j, \Lambda_j$ , and  $\Lambda_j', j=1,2$ , are defined as

$$\begin{aligned} q_{1,2}^2 &= \{ -(\Upsilon_2 E_1 + \Upsilon_1 E_2) \pm [(\Upsilon_2 E_1 - \Upsilon_1 E_2)^2 + 4\Upsilon_1 \Upsilon_2 H_{12}^{\epsilon_2}]^{1/2} \} / 2\Upsilon_1 \Upsilon_2, \\ \kappa_{1,2}^2 &= \{ -(\Upsilon_2' E_1' + \Upsilon_1' E_2') \pm [(\Upsilon_2' E_1' - \Upsilon_1' E_2')^2 + 4\Upsilon_1' \Upsilon_2' H_{12}^{\epsilon_2'}]^{1/2} \} / 2\Upsilon_1' \Upsilon_2', \\ \Lambda_j &= \Lambda(q_j) = -(\Upsilon_2 q_j^2 + E_2) / H_{12}^{\epsilon_2}, \quad j=1,2 \\ \Lambda_j' &= \Lambda'(\kappa_j) = (\Upsilon_2' \kappa_j^2 + E_2') / H_{12}^{\epsilon_2'}, \quad j=1,2 \end{aligned} \tag{26}$$

with

$$\begin{aligned}
 E_1 &= E_c + E_{b1} + H_{11}^\epsilon - E, \\
 E_2 &= E_c + E_{b2} + H_{22}^\epsilon - E, \\
 E'_1 &= -E_1 - V_h, \\
 E'_2 &= -E_2 - V_h.
 \end{aligned}
 \tag{27}$$

In Eq. (26), the  $+$  ( $-$ ) sign in the curly brackets corresponds to  $q_1^2$  and  $\kappa_1^2$  ( $q_2^2$  and  $\kappa_2^2$ ). In the above equations,  $\psi_i(z)$  is composed of two components,  $\cos(q_1 z)[\sin(q_1 z)]$  and  $\cos(q_2 z)[\sin(q_2 z)]$  in the well region if  $\psi_i(z)$  is an even (odd) function of  $z$ . We will call the first component heavy-hole-like and the second component light-hole-like. Whether  $\psi_i(z)$  is heavy-hole-like or light-hole-like will depend on the relative amplitudes of each component.

To perform numerical calculations, we first solve for  $E_c$  using Eqs. (20) and (21) and then specify  $E_c = E_{cn}$  for  $n=1, 2, 3, \dots$ . For each  $E_{cn}$ , we solve for  $E$  using Eq. (23) if  $\psi_i(z)$  is even and Eq. (25) if  $\psi_i(z)$  is odd. The notation  $nmH$  ( $nmL$ ) represents transitions between electrons in the  $n$ th subband and the heavy (light) hole in the  $m$ th subband. For the parameters of our experimental sample, a GaAs/Ga<sub>1-x</sub>Al<sub>x</sub>As quantum well with  $x=0.3$  and  $L=22$  nm, we have the following:  $\gamma_0=14.925$ ,  $\gamma_1=6.85$ ,  $\gamma_2=2.1$ ,  $\gamma_3=2.9$  in the well region,  $V_e=265.86$  meV,  $V_h=113.94$  meV;  $\gamma'_0=10.87$ ,  $\gamma'_1=5.83$ ,  $\gamma'_2=1.674$ ,  $\gamma'_3=2.417$  in the barrier region from Eq. (14). Equations (20) and (21) yield  $E_{cn}$ :  $E_{c1}=8.677$  meV,  $E_{c2}=34.66$  meV, and  $E_{c3}=77.73$  meV for the conduction subbands. Numerical results for  $E$  and  $\psi_i(z)$  are discussed in Sec. IV and comparisons are made with the experimental data.

### III. EXPERIMENT

The sample used in this study was grown by molecular-beam epitaxy along the [001] axis of a semi-insulating GaAs substrate approximately 0.5 mm thick. A series of identical GaAs quantum wells (22-nm GaAs layers separated by 15-nm Al<sub>0.3</sub>Ga<sub>0.7</sub>As layers) were grown on top of a 1- $\mu$ m GaAs buffer layer. All of the epitaxial layers were undoped.

The  $2 \times 8$ -mm<sup>2</sup> sample, required for the low-temperature compressive-stress experiment, was carefully cut, using a wire saw, with the long axis along [100]. Care was taken to ensure that the surfaces to which stress was applied (the  $0.5 \times 2$ -mm<sup>2</sup> faces) were smooth and parallel. The sample was mounted at the bottom of a liquid-helium flow-through cryostat and uniaxial stress was applied to it via a stainless-steel push rod, driven by a piston at the top, which exited the sample chamber of the cryostat through an O-ring seal. Nitrogen gas was used to pressurize the piston. An in-line strain gauge was used to monitor the force on the sample. An accurate determination of the uniaxial stress experienced by the sample was obtained by measuring the stress dependence of excitons in the GaAs buffer layer and utilizing it as a calibrat-

ed stress monitor. The absence of any significant broadening of the noninteracting exciton peaks in the presence of stress was taken to be an indication of the uniformity of applied stress.

The energies of the ground state and several higher-energy exciton transitions in the quantum wells were

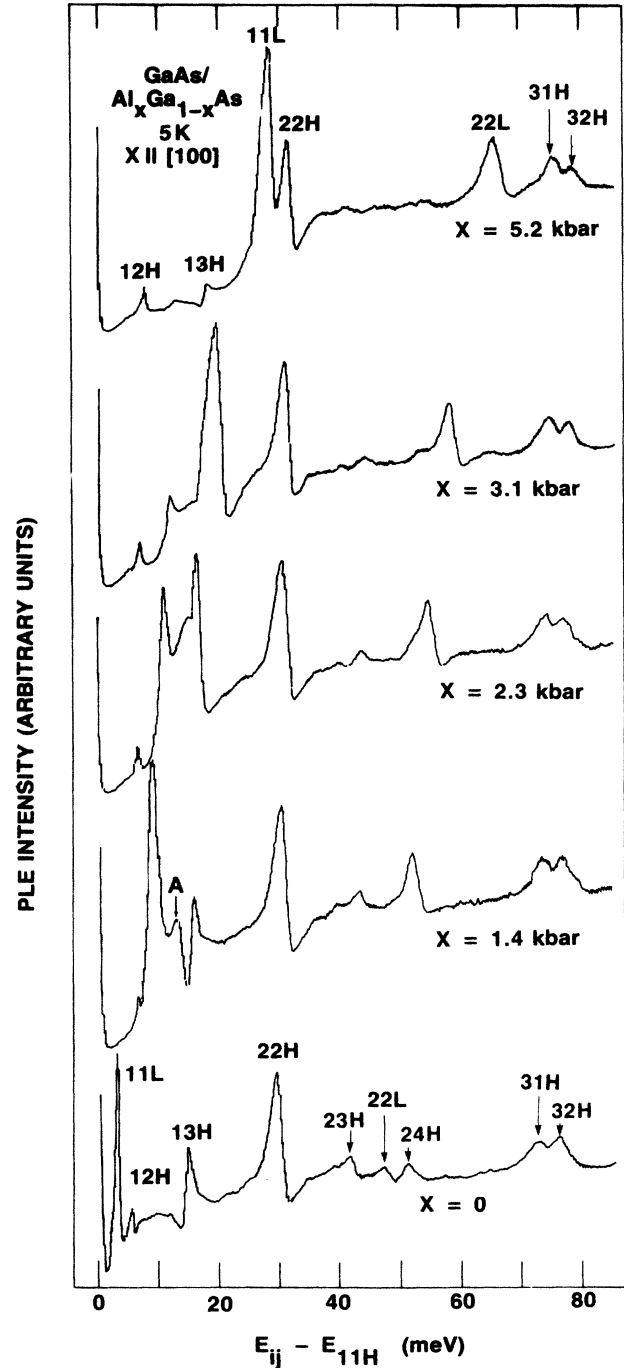


FIG. 1. Low-temperature photoluminescence emission (PLE) spectra of a GaAs/Al<sub>x</sub>Ga<sub>1-x</sub>As multiple quantum well ( $L_z=22$  nm) under five different values of compressive uniaxial stress,  $X \parallel [100]$ . The labels refer to exciton transitions between conduction and valence subbands as explained in the text.  $E_{11H}$  is taken as the origin of the spectra.

determined using low-temperature (5-K) photoluminescence excitation (PLE) spectroscopy. This technique monitors the ground-state PL intensity as a function of exciting laser energy and produces spectra closely analogous to absorption, especially at low temperatures. Typical spectra of a 22-nm GaAs/Al<sub>x</sub>Ga<sub>1-x</sub>As quantum well are presented in Fig. 1. In the bottom and the top curves the peaks in the spectra are labeled according to the notation described in the last section. The spectra in this figure illustrate the changes in exciton energies and oscillator strengths observable as compressive uniaxial stress is applied along the [100] axis. As we shall see later, in this orientation the energies of the light-hole (LH) excitons increase with stress several times more rapidly than do heavy-hole excitons. In order to clarify and emphasize this distinction, the spectra in Fig. 1 were plotted with respect to the ground-state heavy-hole (HH) exciton energy  $E_{11H}$ . Then, in comparing these spectra, it is easy to distinguish features associated with HH excitons (which, as the stress is increased, are stationary or slowly varying in energy with respect to  $E_{11H}$ ) from those associated with LH excitons (which increase their energy rap-

idly from spectrum to spectrum as the stress is increased). Thus, for example, the peak labeled 22L is observed to move quickly to higher relative energies as the stress is increased from 0 to 5 kbar while those labeled 31H and 32H remain almost fixed in relative energy.

This anisotropic sensitivity to stress is observable, perhaps somewhat more clearly, in Fig. 2 in which the energies of the features are plotted as a function of uniaxial stress  $X$ . Again, the peak energies are measured with respect to  $E_{11H}$ . The solid circles are the experimental data and the solid lines are the results of the calculations described above. Again, it is clear that the LH excitons increase in energy more rapidly than HH excitons.

Valence-subband interactions can occur when LH- and HH- exciton states overlap in energy. Experimental evidence for this occurring is in the observation of level repulsion (in which the energies of two states approach each other as  $X$  is increased and then are observed to move away from each other without ever crossing) and oscillator-strength transfer between these two states near the "distance of closest approach."

These points, and the comparison of experimental data with numerical calculations, will be discussed in greater detail in the next section.

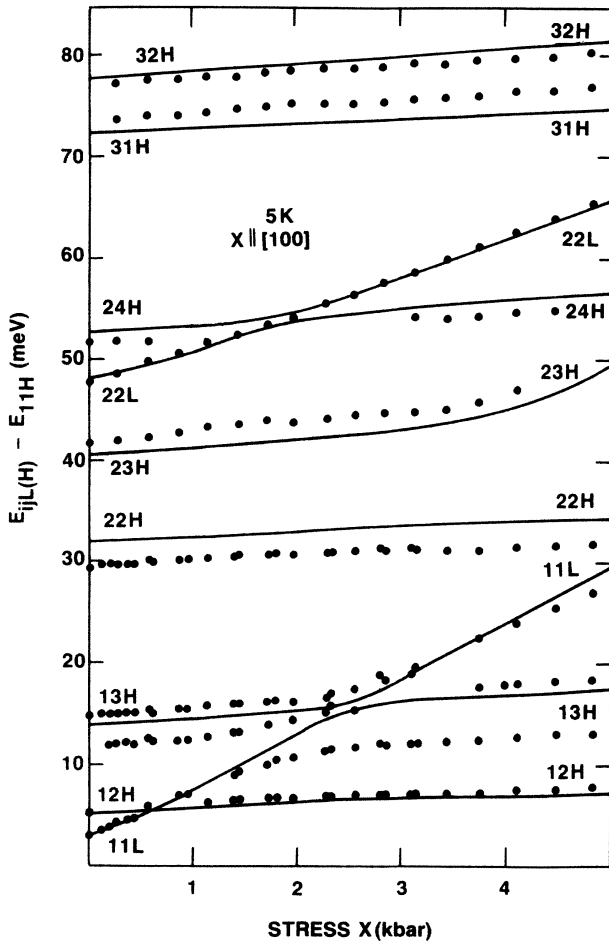


FIG. 2. The uniaxial stress dependencies of higher-energy exciton transitions with respect to  $E_{11H}$ . The solid circles are the experimental data and the solid lines represent the theoretical predictions (see text).

#### IV. RESULTS AND DISCUSSION

In this section the energy  $E_{nmL(H)}$  and wave functions  $\psi_i(z)$  are numerically calculated for two specific directions of stress.

*Case I:  $X \parallel [001]$ .* For  $X \parallel [001]$ , i.e., along the quantization axis  $z$ , the strain matrix elements [Eqs. (8)–(11)] are given by

$$\begin{aligned} H_{11}^\epsilon &= (\eta - 2\delta)X, \\ H_{22}^\epsilon &= (\eta + 2\delta)X, \\ H_{12}^\epsilon &= 0 \end{aligned} \quad (28)$$

with

$$\begin{aligned} \eta &= (D_d + C_1)(2S_{12} + S_{11}), \\ \delta &= \frac{D_u}{3}(S_{12} - S_{11}), \end{aligned} \quad (29)$$

where  $\epsilon_{xx} = \epsilon_{yy} = S_{12}X$ ,  $\epsilon_{zz} = S_{11}X$ , and  $\epsilon_{ij} = 0$  for  $i \neq j$ .  $S_{ij}$  are the coefficients of the elastic compliance tensor and their numerical values for GaAs are listed in Ref. 15. The values for  $D_u$  and  $(D_d + C_1)$  used in our calculations are chosen to be  $-8.23$  and  $-2.75$  eV, respectively to fit the experimental data and are in agreement with our earlier results.<sup>7</sup> In our notation, a negative  $X$  indicates compression. Since  $H_{12}^\epsilon = 0$ , the wave functions in Eq. (16) are decoupled and the envelope functions  $\psi_1(z)$  and  $\psi_2(z)$  represent pure heavy- and light-hole states, respectively. That is, there is no valence-band mixing at  $k = 0$  and the total energy  $E$  is a linear function of  $X$ , as is shown in Fig. 3. In this figure transitions corresponding to the heavy-hole excitons move faster with  $X$  than those of light-hole excitons. Consequently,  $E_{11H}$  and  $E_{11L}$  intersect at  $X = 0.54$  kbar (for  $L_z = 22$  nm). However,

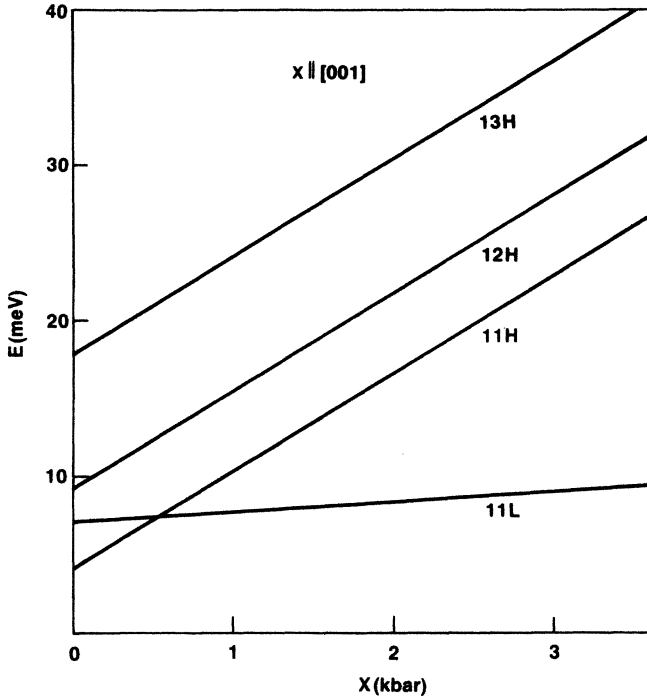


FIG. 3. The calculated energies of exciton transitions,  $E_{ijL(H)}$ , as a function of compressive uniaxial stress, when the stress is along the growth axis,  $X \parallel [001]$ .

valence-band mixing does not occur since the strain Hamiltonian is diagonal. Further, the probability densities are independent of  $X$  because the strain energies do not change the barrier heights  $V_e$  and  $V_h$ .

**Case II.  $X \parallel [100]$ .** When  $X \parallel [100]$ , the strain matrix elements of Eqs. (8)–(11) are

$$\begin{aligned} H_{11}^\epsilon &= (\eta + \delta)X, \\ H_{22}^\epsilon &= (\eta - \delta)X, \\ H_{12}^\epsilon &= \sqrt{3}\delta, \end{aligned} \quad (30)$$

where  $\eta$  and  $\delta$  are defined in Eq. (29). This situation corresponds to our experimental configuration, the results of which were presented in Fig. 2. The solid lines in this figure are the calculated values of  $E_{mnl(H)}$  as a function of  $X$ . Even though, in the theoretical computations, no effort was made to adjust the parameters to maximize the fit, the overall agreement between the experimental data and the calculated curves is very good.

As experimentally observed, the theory predicts that the energies of the LH excitons increase more rapidly with  $X$  than those of HH excitons. This is in contrast to the case of  $X \parallel [001]$  and is a consequence of the change in sign of the  $\delta$  terms in  $H_{11}^\epsilon$  and  $H_{22}^\epsilon$  as can be seen by comparing Eqs. (29) and (30) for the two different directions of applied stress. Thus  $E_{11H}$  and  $E_{11L}$  move apart from one another when compressive stress is applied along  $[100]$  and never intersect. However, the ground state of the LH exciton and some of its higher-energy states can overtake and overlap some of the slower-moving higher

HH exciton states. Thus, for example, in this 22-nm quantum-well sample,  $E_{11L}$  intersects  $E_{12H}$  at about 0.62 kbar and  $E_{13H}$  at about 2.5 kbar.

In the model outlined in Sec. II,  $E_{11L}$  and  $E_{12H}$  are calculated from two decoupled equations [Eqs. (23) and (25)] because of parity arguments. Thus the theory predicts no valence-subband mixing between these two states. On the other hand, the theory predicts a strong mixing between  $E_{11L}$  and  $E_{13H}$  which produces a level repulsion (or “anticrossing”) between these states at about 2.5 kbar. The curves for  $E_{11L}$  and  $E_{13H}$  in Fig. 2 were calculated using Eq. (23) and the even envelope functions  $\psi_i(z)$ . This mixing of the  $1L$  and  $3H$  wave functions is a consequence of the nonzero off-diagonal element  $H_{12}^\epsilon$  in Eq. (16). The result is that the hole wave function  $\psi_i(z)$  is the sum of two components, the  $\cos(q_1z)$  and  $\cos(q_2z)$  terms in Eq. (22), which are heavy- and light-hole-like, respectively. The amplitudes of these two components and therefore the character of the resulting states vary continuously with  $X$ . This is illustrated in the next four figures in which the probability densities  $\rho_i$  for the  $1H$ ,  $1L$ , and  $3H$ , states are shown for three different values of stress.

In Fig. 4, at  $X=0$ , the probability densities for the  $1H$  state are  $\rho_1(z) = |\psi_1(z)|^2$  and  $\rho_2(z) = |\psi_2(z)|^2 = 0$ .  $\rho_1(z)$  is HH-like because only the  $\cos(q_1z)$  term exists. However, when the stress is increased (to 2 and 4 kbar in Fig. 4), although  $\rho_1$  decreases and  $\rho_2$  increases, both remain HH-like with maxima at  $z=0$ . The situation for the  $1L$  state is quite different as is shown in Fig. 5. At  $X=-2$  kbar,  $\rho_2$  decreases and  $\rho_1$  increases. However, both remain LH-like. With  $X=4$  kbar,  $\rho_2(z)$  is smaller still and  $\rho_1(z)$  dominates and now has HH-like characteristics. A similar but opposite transformation takes place for the  $3H$  state as is illustrated in Fig. 6. In this case, at  $X=0$ ,  $\rho_2(z)=0$  and  $\rho_1(z)$  is the dominant wave function.  $\rho_1(z)$  is HH-like. As  $X$  is increased,  $\rho_2(z)$  increases and dominates when  $X > 2$  kbar. At these stresses it has LH-like character and, in fact, is similar to the  $1L$  state at small stresses. (See, for example, Fig. 3.) This is in good qualitative agreement with the experimental data in which  $E_{11L}$  and  $E_{13H}$  exhibit an energy-level repulsion and oscillator-strength transfer at  $X \approx 2.5$  kbar (Figs. 1 and 2).

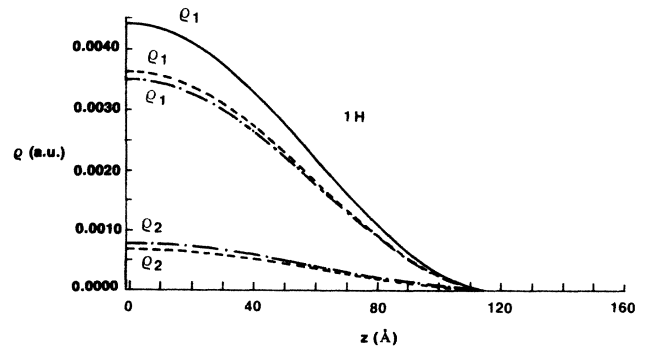


FIG. 4. Probability densities for the  $1H$  state for three different values of stress. The solid, dashed, and dash-dotted curves correspond to  $X=0, 2,$  and  $4$  kbar, respectively.

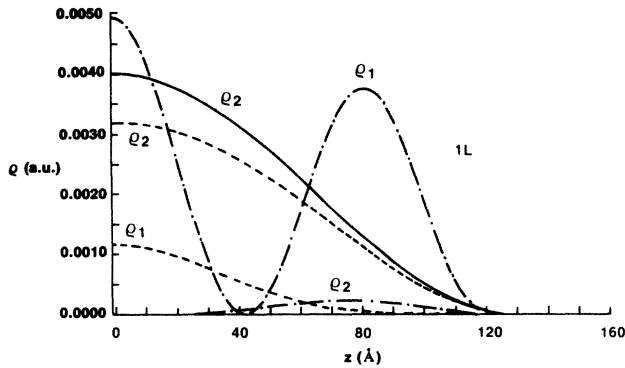


FIG. 5. Probability densities for the  $1L$  state for three different values of stress. The solid, dashed, and dash-dotted curves correspond to  $X=0, 2,$  and  $4$  kbar, respectively.

The main discrepancy between the experiment and theory lies in the experimental observation that, as the stress is increased, the state which began as  $E_{11L}$  appears to approach an energy somewhat below that of  $E_{13H}$  (which the theory predicts should be the asymptotic value). Possible explanations for this unusual behavior are based on processes not included in our theoretical model. For example, our model includes only ground-state excitons and neglects their excited states. Previously, it has been suggested that normally forbidden transitions can give rise to some anomalous features observed in the PLE spectra of QW's. In this picture, the close proximity of a strong, allowed transition, such as  $E_{11L}$ , produces an increase in the oscillator strength of a normally forbidden transition, such as  $E_{12H}$ . The same argument may also be applied to the excited levels of  $E_{12H}$ , which are expected to occur at energies slightly lower than  $E_{13H}$  in this sample. This may be the source of feature *A* in Figs. 1 and 2. Thus  $E_{11L}$  crosses and interacts with several closely spaced states near  $E_{13H}$  and not with just  $E_{13H}$  alone. In this picture, at large  $X$ ,  $E_{11L}$  asymptotically approaches not  $E_{13H}$ , but rather the excited states of  $E_{12H}$ , while these levels approach  $E_{13H}$ . Another possible explanation is based on the fact that our calculations only deal with transitions at the Brillouin-zone center, i.e.,  $k=0$ . This is usually acceptable since densities of states for transitions between the conduction

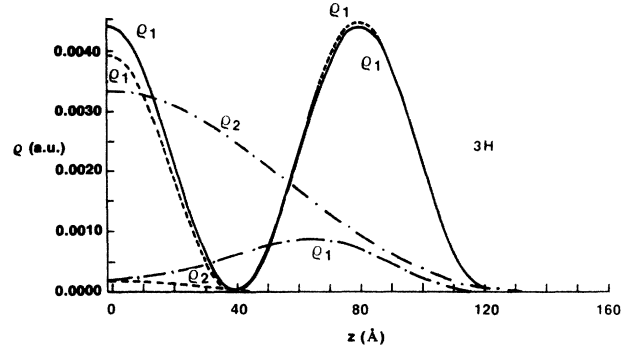


FIG. 6. Probability densities for the  $3H$  state for three different values of stress. The solid, dashed, and dash-dotted curves correspond to  $X=0, 2,$  and  $4$  kbar, respectively.

and valence bands normally have maxima at this point. However, as discussed above, when level repulsion occurs, the wave functions and the energy bands of the interacting levels are strongly distorted. It is conceivable that, under these circumstances, valence energy bands could parallel that of the conduction band over some portion of reciprocal space. Vertical transitions between these bands would result in relatively constant transition energies, i.e., the densities of states for these transitions would possess a peak due to processes taking place away from the zone center. Thus, in this model, the asymptotic energy that  $E_{11L}$  approaches would be due to vertical transitions taking place over some portion of the reciprocal space away from the zone center and thus would not be predicted by our theory. The validity of this model, or of any other explanation, awaits further calculations and experiments on QW's with different thicknesses.

In conclusion, we have presented experimental evidence and theoretical calculations of the mixing of the heavy- and light-hole subbands in GaAs/ $\text{Al}_x\text{Ga}_{1-x}\text{As}$  quantum wells subjected to external uniaxial stress along the [100] axis. The agreement between theory and experiment is good with the exception of the magnitude of the level repulsion experienced by  $E_{11L}$  and  $E_{13H}$ . The theory predicts no valence-subband mixing for stress applied along the [001] direction.

<sup>1</sup>D. S. Chemla, *Helv. Phys. Acta* **56**, 607 (1983).

<sup>2</sup>D. A. B. Miller, D. S. Chemla, P. W. Smith, A. C. Gossard, and W. T. Tsang, *Appl. Phys. B* **28**, 96 (1984).

<sup>3</sup>R. C. Miller, A. C. Gossard, G. D. Sanders, and Y. C. Chang, *Phys. Rev. B* **32**, 8452 (1985).

<sup>4</sup>Emil S. Koteles, C. Jagannath, Johnson Lee, Y. J. Chen, B. S. Elman, and J. Y. Chi, in *Proceedings of the 18th International Conference on the Physics of Semiconductors, Stockholm, 1986*, edited by Olof Engstrom (World-Scientific, Singapore, 1987), p. 625.

<sup>5</sup>R. Sooryakumar, A. Pinczuk, A. C. Gossard, D.S. Chemla, and L. J. Sham, *Phys. Rev. Lett.* **58**, 1150 (1987).

<sup>6</sup>L. Viña, R. Collins, E. E. Mendez, and W. I. Wang, *Phys. Rev. Lett.* **58**, 832 (1987).

<sup>7</sup>C. Jagannath, Emil S. Koteles, Johnson Lee, Y. J. Chen, B. S. Elman, and J. Y. Chi, *Phys. Rev. B* **34**, 7027 (1986).

<sup>8</sup>J. M. Luttinger and W. Kohn, *Phys. Rev.* **97**, 869 (1955).

<sup>9</sup>R. L. Aggarwal, in *Semiconductors and Semimetals*, edited by R. K. Willardson and A. C. Beer (Academic, New York, 1972), Vol. 9, p. 184.

<sup>10</sup>U. Ekenberg and M. Altarelli, *Phys. Rev. B* **32**, 3712 (1985).

<sup>11</sup>J. Shulman and Y. C. Chang, *Phys. Rev. B* **31**, 2056 (1985).

<sup>12</sup>D. Broido and L. J. Sham, *Phys. Rev. B* **31**, 888 (1985).

<sup>13</sup>L. I. Schiff, *Quantum Mechanics* (McGraw-Hill, New York, 1955).

<sup>14</sup>S. S. Nedorezov, *Fiz. Tverd. Tela (Leningrad)* **12**, 2269 (1970).

<sup>15</sup>M. Chandrasekhar and F. H. Pollak, *Phys. Rev. B* **15**, 2127 (1977).